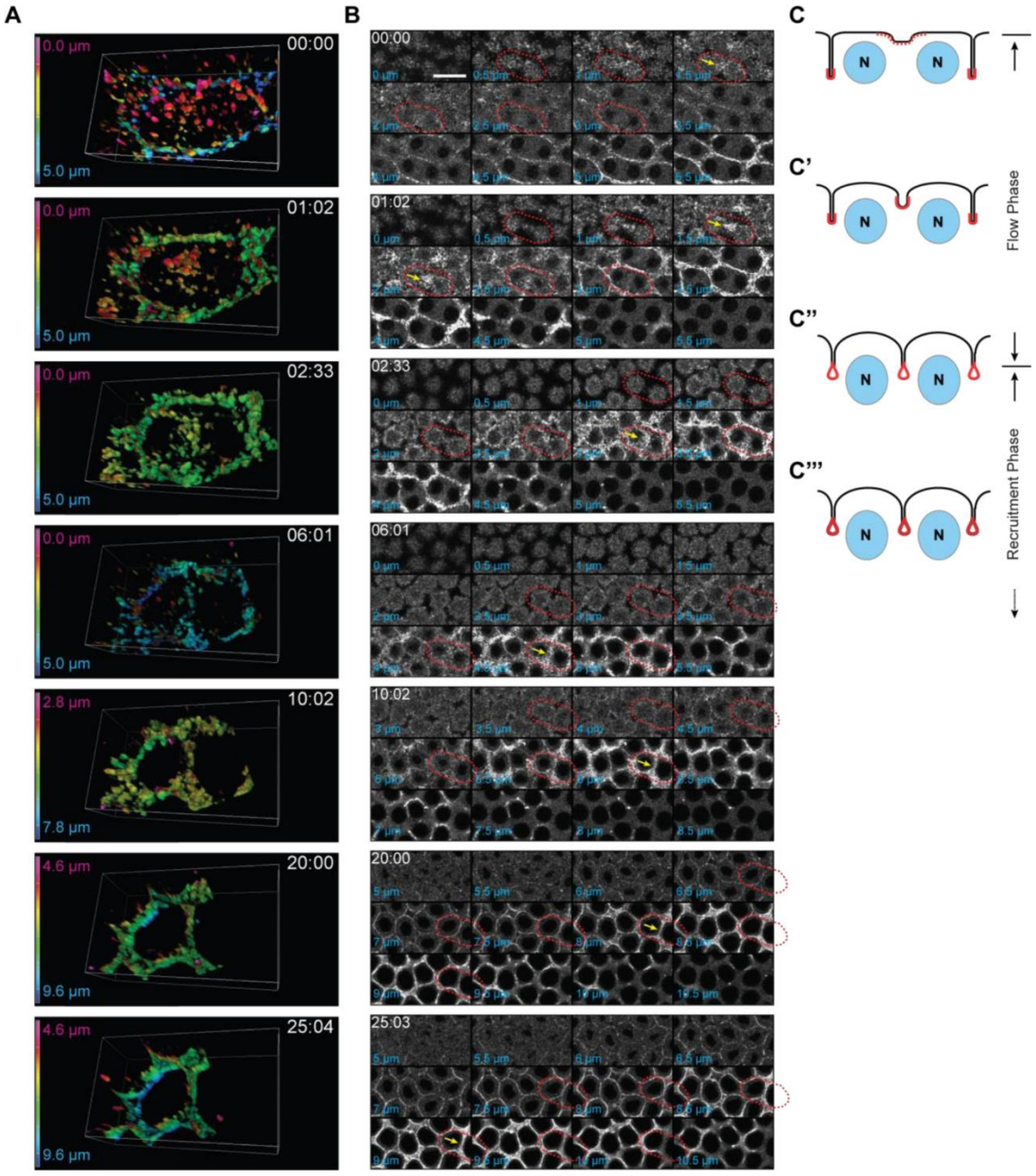

Figure S1. Myosin recruitment to the invagination front during cellularization. (A) Enlarged image of Fig. 1D showing 3D rendering of Sqh-GFP movies during early cellularization. **(B)** Composite images showing myosin from apical to basal planes at various times after the onset of cellularization. Red dotted lines highlight the pair of daughter nuclei shown in Figure 1. Yellow arrow marks the new edge between the two daughter nuclei. Scale bar: 10 µm. **(C-C'')** Schematic diagrams showing the two phases of myosin recruitment from the midsagittal view. Red: myosin. N: nucleus. (C): at beginning of cycle 14, myosin reappears at the tip of the retracting metaphase furrows. Shortly afterwards, myosin puncta appear at the apical cortex, being more concentrated near the equator where the new furrow is forming. (C'): as the new furrow invaginates, myosin flows towards and becomes enriched at the base of the furrow. Meanwhile, the old furrows retract. (C''): the old and new furrows reach the same depth. (C'''): During the recruitment phase, additional myosin is directly recruited from the cytoplasm to the invagination front without undergoing cortical flow.

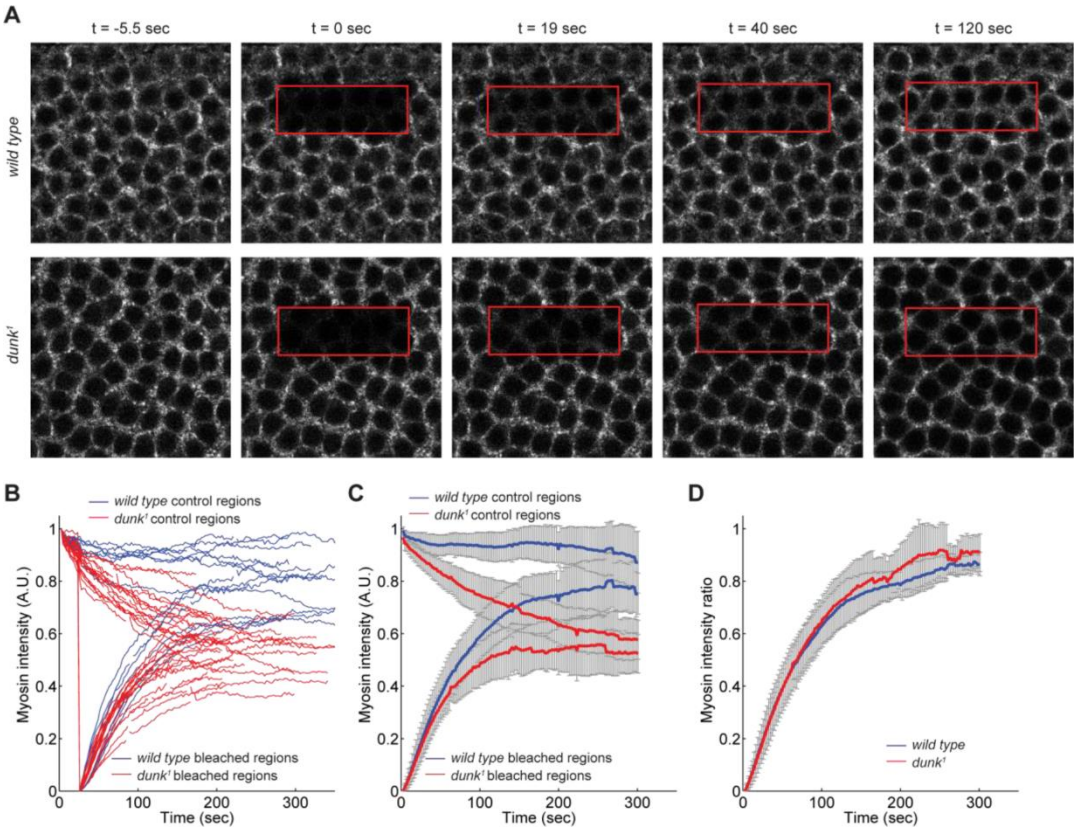

Figure S2. FRAP analysis of cortical myosin dynamics during the flow phase. (A) Photo-bleaching and recovery of Sqh-GFP at invagination front during cellularization at the flow phase. Boxed region was bleached at $t = 0$. **(B)** Quantification of myosin intensity at the invagination front. Top curves: unbleached control regions. Bottom curves: bleached regions. Blue curves: wild type embryos ($n = 7$ embryos). Red curves: *dunk*^{1} mutant embryos ($n = 16$ embryos). **(C)** Average myosin intensity in wild type and *dunk*^{1} mutant embryos. Error bars: s.d. **(D)** Average ratio between myosin intensities measured at the bleached region and the control region. Error bars: s.d.

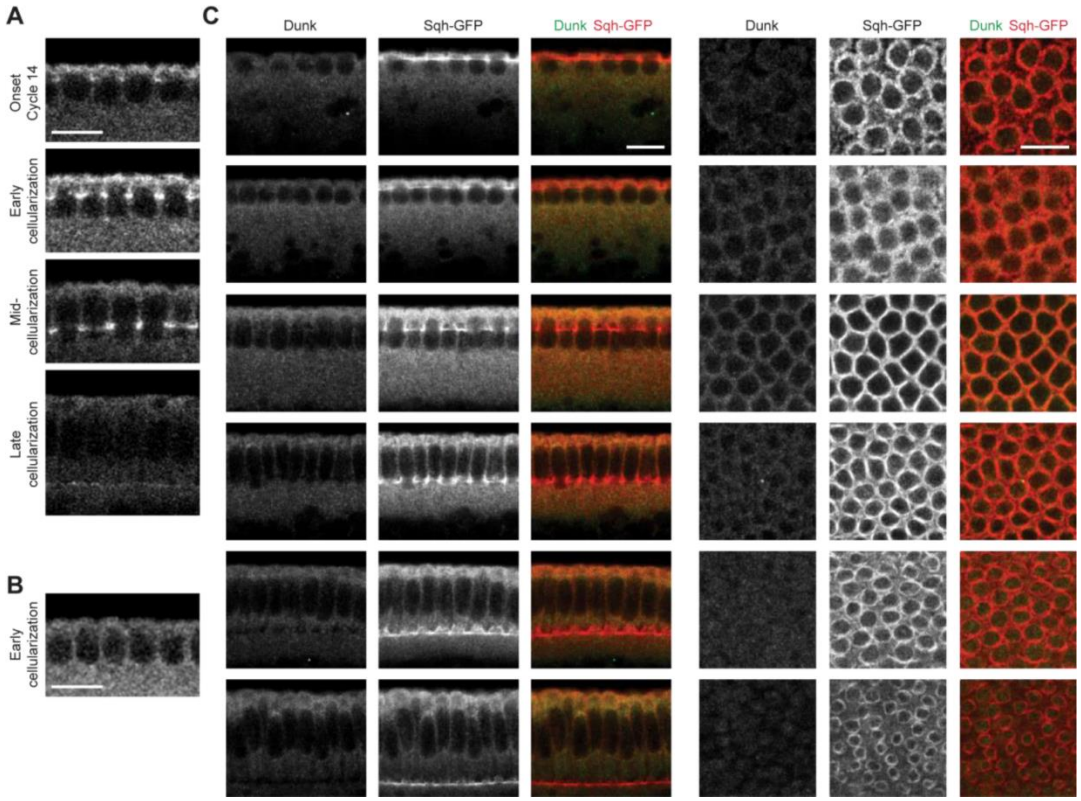

Figure S3. Immunostaining of Dunk in Oregon R and *dunk*^{1} mutant embryos. (A) Immunostaining of wild type Oregon R embryos with anti-Dunk antibodies. Dunk specifically localizes to invagination front during early cellularization. Scale bar: 10 µm. **(B)** Immunostaining of *dunk*^{1} mutant embryos with anti-Dunk antibodies. Scale bar: 10 µm. **(C)** Immunostaining of *dunk*^{1}*; sqh-GFP* embryos with anti-Dunk and anti-GFP antibodies. Left panel: mid-sagittal view; Right panel: en face view. Scale bar: 10 µm.

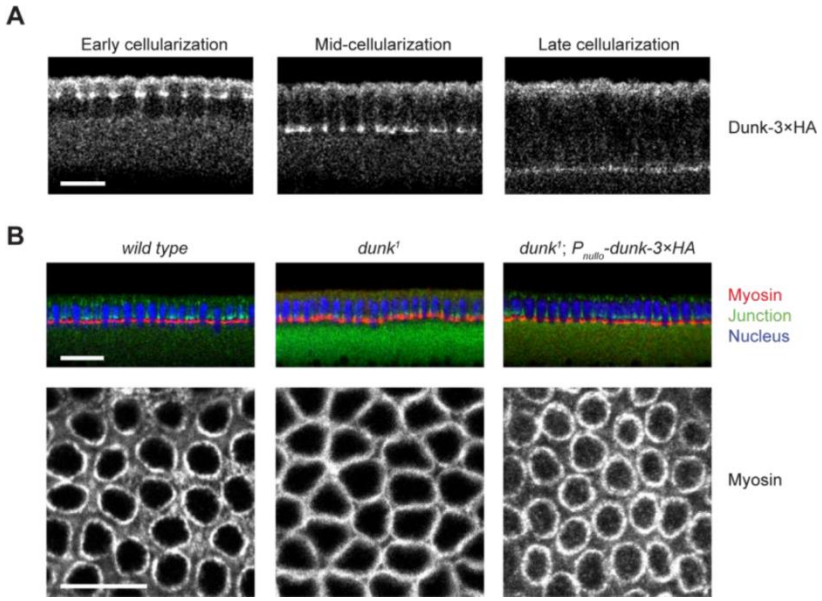

Figure S4. Rescue of the *dunk*^{1} mutant phenotype with the P_{nullo}-*dunk-3×HA* transgene. (A) Immunostaining of *dunk*^{1}*;* P_{nullo}*-dunk-3×HA* embryos with anti-HA antibodies. Dunk-3×HA shows similar localization as endogenous Dunk. Scale bar: 10 µm **(B)** Top: Cross sections of *wild type*, *dunk*^{1} or *dunk*^{1}*;* P_{nullo}*-dunk-3×HA* embryos showing staining of β-catenin (green), myosin (red) and DNA (blue); Scale bar: 20 µm; bottom: En face view showing myosin staining at the invagination front. Scale bar: 10 µm. Expression of *dunk-3×HA* under the control of P_{nullo} rescues the myosin phenotype in *dunk*^{1} mutant embryos.

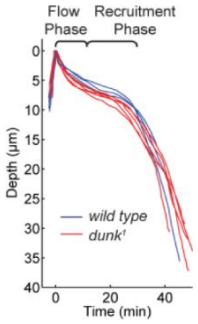

Figure S5. *dunk*^{1} mutant embryos show no defects in the rate of furrow ingression. Shown is the depth of invagination front (marked by Sqh-GFP) as a function of time. Each line represents one embryo. Wild type: $n = 3$; *dunk*^{1}: $n = 5$.

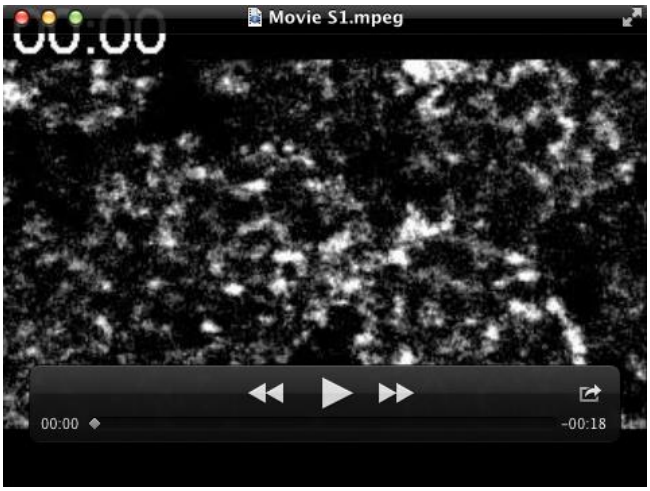

Movie S1: Projections of confocal sections showing Sqh-GFP at the invagination front in wild type embryos. Shown is a single pair of daughter nuclei at the beginning of cellularization. The time format is MM:SS in all movies. *t* = 0 marks the beginning of cellularization in all movies unless stated otherwise.

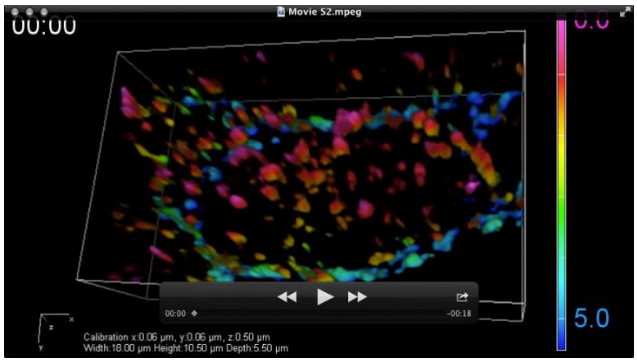

Movie S2: 3D rendering of the Sqh-GFP movie that corresponds to Movie S1, showing a single pair of daughter nuclei at the beginning of cellularization. Color-coding corresponds to the depth of myosin structures from the apical surface (unit: µm).

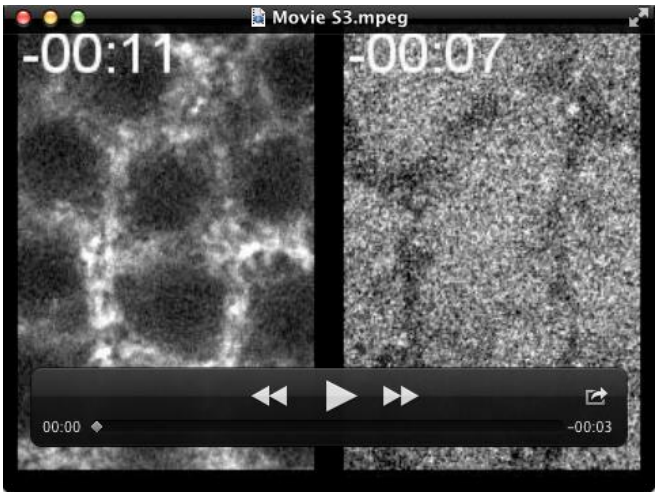

Movie S3: Left: Laser ablation of a newly formed cleavage furrow in an embryo expressing Sqh-GFP. Right: Laser ablation in an embryo at cycle 13 anaphase. *t = 0* marks the time of ablation.

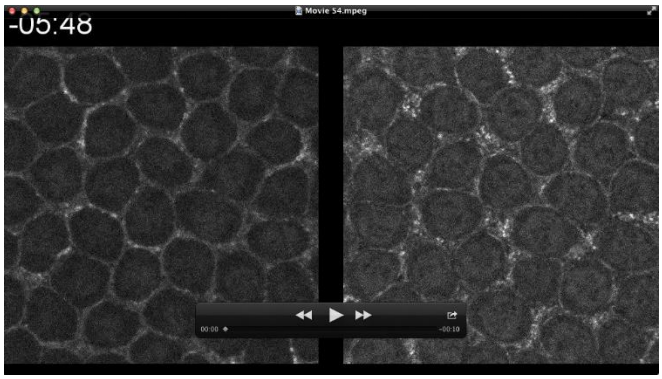

Movie S4: Comparing Sqh-GFP in wild type (left) and *dunk*^{1} mutant (right) embryos. Shown are projections of confocal sections at the invagination front.

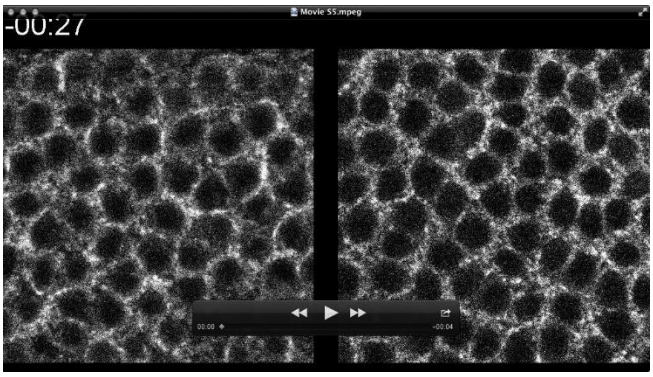

Movie S5: FRAP analysis of Sqh-GFP in wild type (left) and *dunk*^{1} mutant (right) embryos. t = 0 marks the time of photo-bleaching.

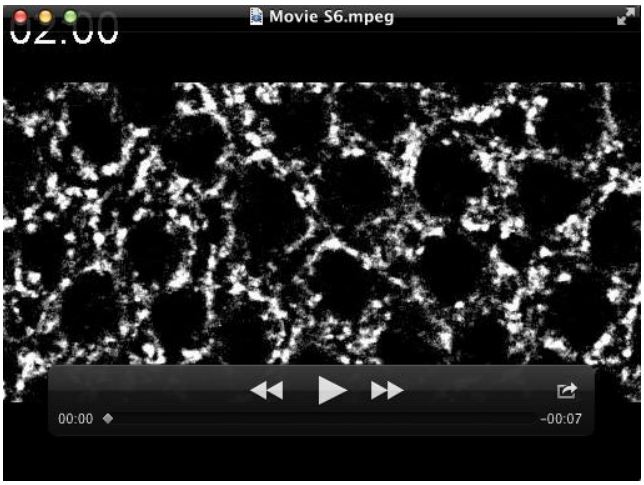

Movie S6: Projections of confocal sections showing Sqh-GFP at the invagination front in *dunk*^{1} mutant embryos. The movie begins at approximately 2 min after the onset of cellularization as estimated based on the morphology of the actomyosin network.

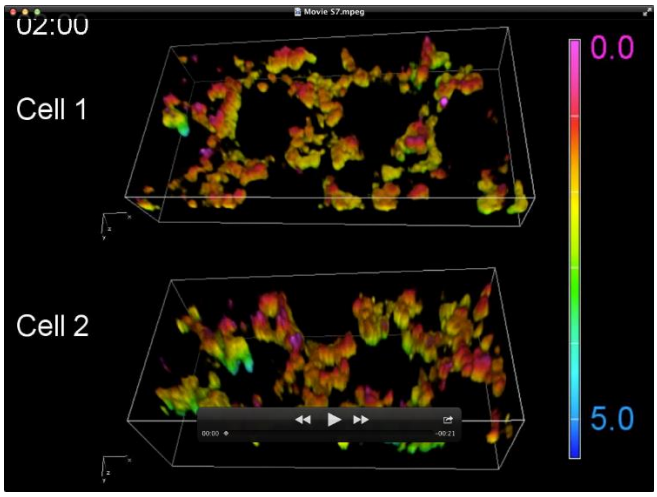

Movie S7: 3D rendering of the Sqh-GFP movie that corresponds to Movie S6. Shown are two pairs of daughter nuclei as examples. Color-coding corresponds to the depth of myosin structures from the apical surface (unit: µm).

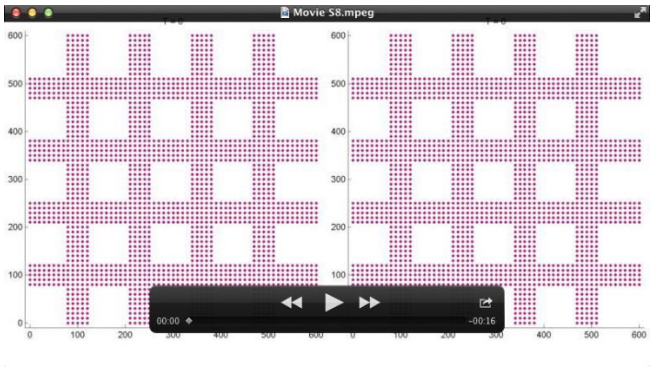

Movie S8: Computer simulation of an interconnected contractile network. Left: $k_{on} >> k_{off}$ ($[k_{on}, k_{off}] = [0.05, 0.001]$). Right: $k_{on} \sim k_{off}$ ($[k_{on}, k_{off}] = [0.003, 0.001]$). Red: myosin nodes; Blue: membrane nodes (See supplementary methods for details).

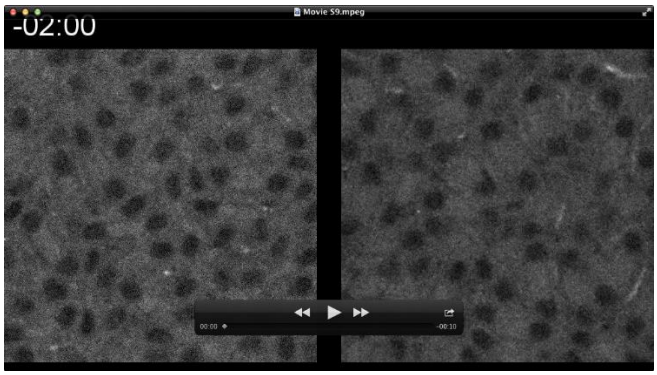

Movie S9: Comparing Sqh-GFP in *slam* (left) and *slam dunk*^{1} (right) mutant embryos. Shown are projections of confocal sections at the invagination front.

Supplementary Methods

Computer simulation of a contractile network

In order to demonstrate how tension drives anisotropic myosin flow and how myosin turnover at the cortex affect the mechanics of the network, we generated a computer model to simulate the behavior of an interconnected contractile network. The source code for image analysis and computational modeling is available to download as a MATLAB M-file (Computer_vertex_model_final).

(1) Components of the model

During cellularization, the rearrangement of the actomyosin structures is largely confined at the plane of the invagination front. We therefore took a simplified approach to only consider a contractile network on a 2-dimensional plane. Our model contains two components. The active component represents the actomyosin contractile network, and the passive component corresponds to the membrane cortex that can be stretched by actomyosin contractions but will also provide weak resistance. In embryos, the actomyosin network is associated with the membrane cortex through molecular anchors. In our model, the active and passive components are connected by springs to reflect the anchorage of the actomyosin network to the cortex.

(1a) Passive component

We modeled the membrane cortex as a two-dimensional plane tiled into a 60 × 60 grid of squares, with a membrane node sits at each intersection of the grid. The initial size of each square is $L_0 \times L_0$. We assumed that the actin cortex lining underneath the membrane provide the invagination front elastic properties that will resist deformations caused by active constrictions. We implemented this by providing elastic restoring forces that prevent the movement of the membrane nodes relative to their neighbors. The force is expressed as:

$$F_x = \mu_b(|x - x'| - |x_0 - x_0'|)$$

$$F_y = \mu_b(|y - y'| - |y_0 - y_0'|)$$

where μ_b is the relative "spring constants" of the restoring forces. For the two neighboring nodes: x and x' are the current x position, x_0 and x_0' are the original x position, y and y' are the current y position, and y_0 and y_0' are the original y position. The presence of the elastic, non-constricting regions covering the entire basal plane reflects our assumption that both the apical-lateral cortex and the invagination front (basal cortex) could resist the pulling from the basal actomyosin network although they are not exactly positioned at the same apical-basal depth.

(1b) Active component

We implemented myosin contractility by defining an interconnected contractile network that overlaps the membrane mesh grid. The contractile network is composed of 4 vertical and 4 horizontal stripes of squares, each of which is 4-square wide and 9-square apart from its neighboring stripe (Fig. 6A). The overlapping regions of vertical and horizontal stripes represent the vertices of the network, whereas the non-overlapping regions represent the edges. In the model each edge or vertex contains multiple constricting interfaces, initially spaced broadly to reflect the initial meshwork-like appearance of the actomyosin cytoskeleton. The pulling force exerted by a neighboring myosin node is expressed as:

$$F_x = \mu_a(|x - x'|)$$

$$F_y = \mu_a(|y - y'|)$$

where μ_a is the relative "spring constants" of the interfaces between neighboring myosin nodes. For the two neighboring nodes: x and x' are the current x position, y and y' are the current y position.

(1c) Connections between myosin nodes and membrane nodes

To reflect physical interactions between cortical myosin and the membrane cortex, we defined the connection between the myosin nodes and their overlapping membrane nodes by assigning a spring-like force that resists the separation of the two. The spring like force is expressed as:

$$F_x = \mu_c(|x - x'|)$$

$$F_y = \mu_c(|y - y'|)$$

where μ_c is the relative "spring constants" of the interfaces between the myosin nodes and their corresponding membrane nodes. For each pair of myosin node and membrane node: *x* and *x'* are the current x position, *y* and *y'* are the current y position, respectively.

(1d) Boundary conditions

In the actual embryo, the basal actomyosin network is formed across the entire invagination front and does not have an effective boundary. We therefore restrained the nodes located at the boundary of the mesh grid from moving out of the boundary.

(2) Implementation of myosin turnover in the simulation

We implemented myosin turnover dynamics in the simulation by the following approach. For each simulation step, a fraction (determined by k_{off}) of myosin nodes, randomly selected, are eliminated from the network, resembling the dissociation of myosin from the cortex. Once a myosin node disappears, the interfaces connecting the node and its neighbors disappear altogether. Subsequently, myosin nodes will reappear at a random fraction (determined by k_{on}) of the membrane nodes, resembling the recruitment of myosin to the cortex. Once a myosin node reappears, the interfaces connecting the node and its neighbors, if still present, are also reestablished.

(3) Energy equations

(3a) The energy status of a myosin node (*i*,*j*) is given by:

$$E(x_{i,j}, y_{i,j}) = \frac{\mu_a}{2}(G^2_{i-1,j} + G^2_{i+1,j} + G^2_{i,j-1} + G^2_{i,j+1}) + \frac{\mu_c}{2}(H^2_{i,j})$$

$$G^2_{i-1,j} = (x_{i,j} - x_{i-1,j})^2 + (y_{i,j} - y_{i-1,j})^2$$

$$G^2_{i+1,j} = (x_{i,j} - x_{i+1,j})^2 + (y_{i,j} - y_{i+1,j})^2$$

$$G^2_{i,j-1} = (x_{i,j} - x_{i,j-1})^2 + (y_{i,j} - y_{i,j-1})^2$$

$$G_{i,j+1}^2 = (x_{i,j} - x_{i,j+1})^2 + (y_{i,j} - y_{i,j+1})^2$$

$$H_{i,j}^2 = (x_{i,j} - x'_{i,j})^2 + (y_{i,j} - y'_{i,j})^2$$

Therefore,

$$\frac{dE(x_{i,j}, y_{i,j})}{dx_{i,j}} = \mu_a \left((x_{i,j} - x_{i-1,j}) + (x_{i,j} - x_{i+1,j}) + (x_{i,j} - x_{i,j-1}) + (x_{i,j} - x_{i,j+1}) \right) + \mu_c (x_{i,j} - x'_{i,j})$$

$$\frac{dE(x_{i,j}, y_{i,j})}{dy_{i,j}} = \mu_a \left((y_{i,j} - y_{i-1,j}) + (y_{i,j} - y_{i+1,j}) + (y_{i,j} - y_{i,j-1}) + (y_{i,j} - y_{i,j+1}) \right) + \mu_c (y_{i,j} - y'_{i,j})$$

where $x_{i,j}$ and $y_{i,j}$ denotes the x and y coordinates of the myosin node (i,j). $x'_{i,j}$ and $y'_{i,j}$ denotes the x and y coordinates of the corresponding membrane node (i,j). The coefficients μ_a and μ_c are the relative "spring constants" of the interfaces between neighboring myosin nodes and those between the myosin node and the associated membrane node, respectively.

(3b) The energy status of a membrane node (i,j) is given by:

$$E(x_{i,j}, y_{i,j}) = \frac{\mu_b}{2} G_{i-1,j}^2 + G_{i+1,j}^2 + G_{i,j-1}^2 + G_{i,j+1}^2) + \Phi_{i,j} \frac{\mu_c}{2} (H_{i,j}^2)$$

$$G_{i-1,j}^2 = ((x_{i,j} - x_{i-1,j}) - (x0_{i,j} - x0_{i-1,j}))^2 + ((y_{i,j} - y_{i-1,j}) - (y0_{i,j} - y0_{i-1,j}))^2$$

$$G_{i+1,j}^2 = ((x_{i,j} - x_{i+1,j}) - (x0_{i,j} - x0_{i+1,j}))^2 + ((y_{i,j} - y_{i+1,j}) - (y0_{i,j} - y0_{i+1,j}))^2$$

$$G_{i,j-1}^2 = ((x_{i,j} - x_{i,j-1}) - (x0_{i,j} - x0_{i,j-1}))^2 + ((y_{i,j} - y_{i,j-1}) - (y0_{i,j} - y0_{i,j-1}))^2$$

$$G_{i,j+1}^2 = ((x_{i,j} - x_{i,j+1}) - (x0_{i,j} - x0_{i,j+1}))^2 + ((y_{i,j} - y_{i,j+1}) - (y0_{i,j} - y0_{i,j+1}))^2$$

$$H_{i,j}^2 = (x_{i,j} - x'_{i,j})^2 + (y_{i,j} - y'_{i,j})^2$$

Therefore,

$$\frac{dE(x_{i,j},y_{i,j})}{dx_{i,j}} = \mu_b\Big(\big((x_{i,j}-x_{i-1,j})-(x0_{i,j}-x0_{i-1,j})\big) + \big((x_{i,j}-x_{i+1,j})-(x0_{i,j}-x0_{i+1,j})\big) + \big((x_{i,j}-x_{i,j-1})-(x0_{i,j}-x0_{i,j-1})\big) + \big((x_{i,j}-x_{i,j+1})-(x0_{i,j}-x0_{i,j+1})\big)\Big) + \Phi_{i,j}\mu_c(x_{i,j}-x'_{i,j})$$

$$\frac{dE(x_{i,j},y_{i,j})}{dy_{i,j}} = \mu_b\Big(\big((y_{i,j}-y_{i-1,j})-(y0_{i,j}-y0_{i-1,j})\big) + \big((y_{i,j}-y_{i+1,j})-(y0_{i,j}-y0_{i+1,j})\big) + \big((y_{i,j}-y_{i,j-1})-(y0_{i,j}-y0_{i,j-1})\big) + \big((y_{i,j}-y_{i,j+1})-(y0_{i,j}-y0_{i,j+1})\big)\Big) + \Phi_{i,j}\mu_c(y_{i,j}-y'_{i,j})$$

where $x_{i,j}$ and $y_{i,j}$ denotes the x and y coordinates of the membrane node (i,j). $x'_{i,j}$ and $y'_{i,j}$ denotes the x and y coordinates of the myosin node (i,j). $x0_{i,j}$ and $y0_{i,j}$ denotes the x and y coordinates of the membrane node (i,j) at its original position. μ_b and μ_c are the relative "spring constants" of the interfaces between neighboring membrane nodes and those between the membrane node and the associated myosin node, respectively. $\Phi_{i,j}$ is defined as 1 for membrane nodes that link to a myosin node, and 0 for membrane nodes that does not link to a myosin node.

(3c) Boundary conditions

We restrained the nodes located at the boundary of the mesh grid from moving out of the boundary. For beads located at the vertical boundaries:

$$\frac{dE(x_{i,j},y_{i,j})}{dx_{i,j}} = 0$$

For beads located at the horizontal boundaries:

$$\frac{dE(x_{i,j},y_{i,j})}{dy_{i,j}} = 0$$

(3d) Energy minimum search

We searched for the minimum of our main energy function for a selected small step size *dt*:

$$x_{i,j}(t+dt) = x_{i,j}(t) - \frac{dE(x_{i,j}, y_{i,j})}{dx_{i,j}} dt$$

$$y_{i,j}(t+dt) = y_{i,j}(t) - \frac{dE(x_{i,j}, y_{i,j})}{dy_{i,j}} dt$$

(4) Parameter settings for Figure 6 and Movie S8:

Parameters	***wild type***	***dunk*[1]**
μ_a	1	1
μ_b	0.01	0.01
μ_c	0.5	0.5
L_0	10	10
dt	0.05	0.05
k_{on}	0.05	0.003
k_{off}	0.001	0.001